6 GFP-Expressing Metastatic-Cancer Mouse Models

Robert M. Hoffman, PhD

CONTENTS

INTRODUCTION
METHODS
REFERENCES

1. INTRODUCTION

The visualization of tumor invasion and micrometastasis formation in viable fresh tissue or the live animal is necessary for a critical understanding of tumor progression and its control. However, the visualization of individual tumor cells in vivo has not been possible because of the lack of a sufficient marker. Previous studies used transfection of tumor cells with the *Escherichia coli (E. coli)* beta-galactosidase (lacZ) gene to detect micrometastases *(1,2)*. Detection of lacZ, however, requires extensive histological preparation, and therefore it has not been possible to detect and visualize tumor cells in viable fresh tissue or the live animal at the microscopic level.

To allow visualization of micrometastases in fresh tissue, we have utilized the green fluorescent protein (GFP) gene, cloned from the bioluminescent jellyfish *Aequorea victoria (3)*. GFP has demonstrated its potential for use as a marker for gene expression in a variety of cell types *(4,5)*. The GFP cDNA encodes a 283-amino-acid polypeptide with a mol wt of 27 *Kd (6,7)*. The monomeric GFP requires no other *Aequorea* proteins, substrates, or cofactors to fluoresce *(8)*. Recently, GFP gene gain-of-function mutants have been generated by various techniques *(9–12)*. For example, the GFP-S65T clone has the serine-65 codon substituted with a threonine codon, which results in a single excitation peak at 490 nm *(9)*. Moreover, to develop higher expression in human and other mammalian cells, a humanized hGFP-S65T clone was isolated *(13)*. The much brighter fluorescence in the mutant clones allows for easy detection of GFP expression in transfected cells.

We have isolated more than 50 GFP transfectants of human and animal cancer cells that are stable in vitro and in vivo *(14–19)*. The transfectants are highly fluorescent in vivo in tumors formed from the cells. Using these fluorescent transfectants, orthotopic-transplant animal models *(18–22)* were utilized for visualizing the metastatic processes in fresh tissue down to the single-cell level, as well as by whole-body imaging that was not previously possible.

From: *Tumor Models in Cancer Research*
Edited by: B. A. Teicher © Humana Press Inc., Totowa, NJ

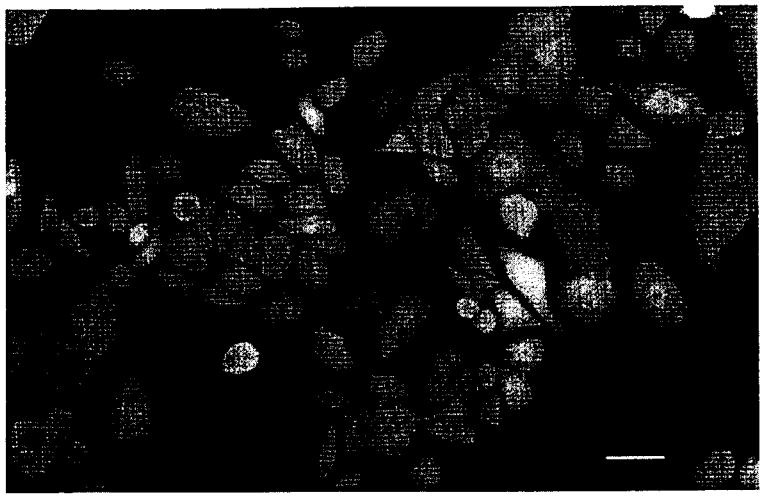

Fig. 1. Confocal micrograph of subclone of lung-cancer-cell line ANIP epxressing GFP in vitro. Cells were transfected with the dicistronic GFP expression vector pED-MTX^r. Cells were selected in methotrexate (MTX). GFP-expressing cells pictured above were able to growth in 50 nm MTX *(15)*.

1.1. Isolation of Stable High-Level Expression GFP Transductant Tumor-cell Lines

For isolation of very bright GFP-expressing tumor cells, the concentration of a selective agent, such as G418, is increased gradually up to 800–1200 μg/ml for selection of clones with increased expression of GFP. Bright GFP clones are then selected in the absence of antibiotic (Fig. 1) as a basis for stable high GFP expression in vivo *(18)*.

The stability of CHO-K1-GFP cells maintained in the presence vs absence of a selective agent over a 24-d period in vitro has been quantified. For cells grown in the presence of the selective agent, the median fluorescence intensity at d 3 was 105 (arbitrary units) compared to 81 *u* at d 24. In the absence of selective agents, cells showed a median fluorescence intensity of 95 *u*, similar to that of cells maintained under selective pressure at d 24. Thus, the GFP expression of the cells was sufficiently stable to permit visualization in vivo, even in the absence of selective pressure. Nonfluorescent cells were not detected among cells maintained with or without selective agents *(28)*.

1.2. GFP-Expressing Macro- and Micrometastases Using CHO Cells in Orthotopic Models

Nude mice were implanted into the ovary with 1-mm^3 cubes of stable-high-GFP-expression CHO-K1, that previously grew subcutaneously in nude mice *(14)*. All mice had tumors in the ovaries. The tumor subsequently spread throughout the peritoneal cavity, including the colon, cecum, small intestine, spleen, and peritoneal wall. The primary tumor and peritoneal metastases were strongly fluorescent. Numerous micrometastases were detected by fluorescence on the lungs of all mice. Multiple micrometastasis were also detected by fluorescence on the liver, kidney, contralateral ovary, adrenal gland, para-aortic lymph node, and pleural membrane down to the sin-

gle-cell level. Single-cell micrometastases could not be detected by standard histological techniques. Even multiple-cell small colonies were difficult to detect by hematoxylin and eosin staining, but they could be detected and visualized clearly through GFP fluorescence.

Chinese homster ovary cells (CHO) proved to be highly metastatic from both the subcutaneous (sc) and orthotopic sites, as brightly visualized by GFP fluorescence. Metastases were visualized by GFP expression in the lung, pleural membrane, spleen, kidney, ovary, adrenal gland, and peritoneum after orthotopic implantation in nude mice. Metastases were visualized by GFP expression, mainly in the lung and pleural membrane after sc implantation in nude mice. Metastases were visualized in the lung and pleural membrane, liver, kidney, and ovary after sc implantation in (SCID) mice *(23)*.

1.3. Patterns of Contralateral and Regional Lung Tumor Metastases Visualized by GFP Expression in Orthotopic Models

The primary tumor grew in the implanted left lung in all mice after surgical orthotopic implantation (SOI) of GFP-transfected ANIP–973. GFP expression allowed visualization of the advancing margin of the tumor spreading throughout the ipsilateral lung. All animals explored had evidence of chest-wall invasion, and local and regional spread. Metastatic contralateral tumors involved the mediastinum, contralateral pleural cavity, and the contralateral visceral pleura. While the ipsilateral tumor had a continuous and advancing margin, the contralateral tumor seems to have been formed by multiple seeding events. These observations were made possible by the stable, high-GFP fluorescence of the tumor cells *(15,16)* (Fig. 1). Contralateral hilar lymph nodes were also involved, as well as cervical lymph nodes visualized by GFP expression *(15,16)*. When non-GFP-transfected ANIP was compared with GFP-transformed ANIP for metastatic capability similar results were seen *(15)*.

1.4. GFP-Expressing Bone Metastases of Lung Cancer in Orthotopic Models

Nude mice were implanted in the left lung by SOI with 1-mm^3 cubes of H460-GFP tumor tissue derived from an H460-GFP sc tumor *(18)*. The implanted mice were sacrificed at 3–4 wk at the time of significant decline in performance status. GFP fluorescence demonstrated metastases in the left lung, the contralateral lung, the chest wall, and the skeletal system. It was determined by GFP fluorescence that the vertebrae (Fig. 2) were the most involved skeletal site of metastasis. Metastasis could also be visualized in the tibia and femur marrow by GFP fluorescence *(18)*.

1.5. Prostate-Cancer Bone and Visceral Metastasis Visualized by GFP in Orthotopic Models

A stable high GFP expression clone of human prostate carcinoma PC-3 was orthotopically implanted surgically in nude mice. Subsequent skeletal metastasis included the skull (Fig. 3), rib, pelvis, femur, and tibia. All the tumors metastasized to the lung, pleural membrane, and kidney. Four of five tumors metastasized to the liver, and two of five tumors metastasized to the adrenal gland. In two mice, cancer cells or small colonies were seen in the brain, and in one mouse, a few cells could be seen in the spinal cord by GFP fluorescence *(19)*.

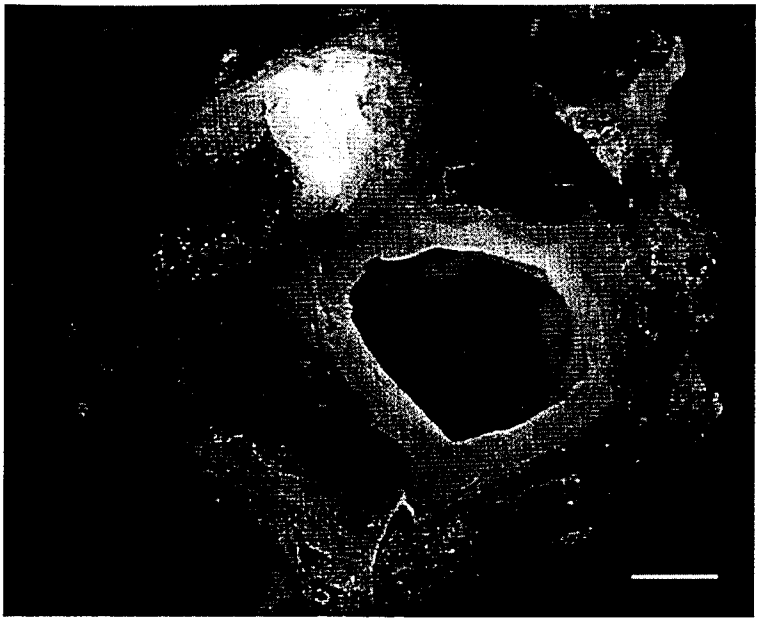

Fig. 2. Lumbar vertebral metastasis in nude mouse after orthotopic transplantation of GFP-expressing human lung-cancer line H-460 transfected with GFP retrovirus pLEIN and selected in G418 *(18)*.

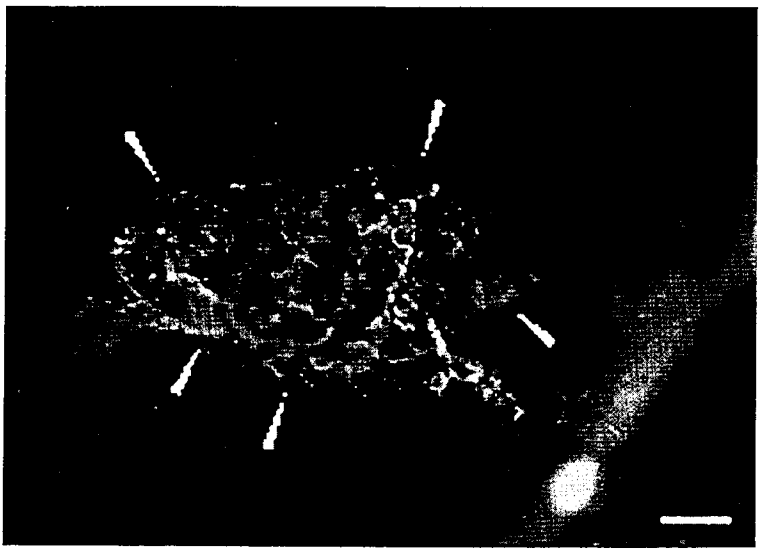

Fig. 3. Skull metastasis of GFP-expressing human prostate carcinoma PC-3 orthotopically transplanted in nude mice. PC-3 was transduced with the GFP retrovirus pLEIN and selected in G418 *(19)*.

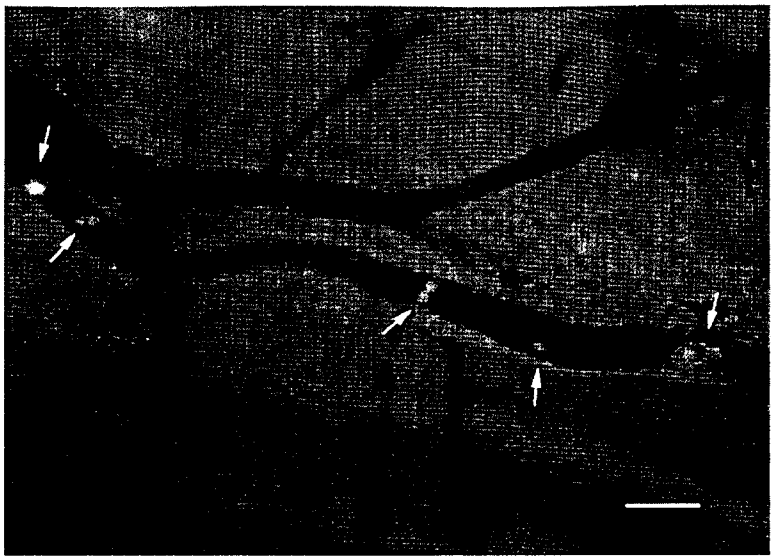

Fig. 4. GFP-expressing CHO-K1 cells in a peritoneal vessel 2 min after tail-vein injection in nude mice. CHO-K1 cells were transduced with the dicistronic GFP vector. pED-MTX^r and selected in MTX *(14)*.

1.6. GFP-Expressing Experimental Metastases in Nude Mice

CHO-K1 GFP transfectants injected via the tail vein were visualized by GFP expression in the peritoneal wall vessels down to the single-cell level *(14)* (Fig. 4). These cells formed emboli in the capillaries of the lung, liver, kidney, spleen, ovary, adrenal gland, thyroid gland, and brain.

ANIP GFP cells were injected into the tail vein of nude mice, which were sacrificed at 4 and 8 wk. In both groups, numerous micrometastatic colonies were detected in the whole-lung tissue by GFP expression in fresh tissue *(16)*. Even 8 wk after injection, in most of the mice colonies were not obviously further developed as compared to mice sacrificed at 4 wk *(16)*. Numerous small colonies, which ranged in size down to less than 10 cells, were detected at the lung surface in both groups. After 8 wk, metastases in the brain (Fig. 5), the submandibular gland, the lung, the pancreas, the bilateral adrenal glands, the peritoneum, and the pulmonary hilum lymph nodes were visualized by GFP expression. Actively colonizing as well as dormant tumor cells were visualized in the lung *(16)*. Dormant micrometastasis is one of the most important steps in tumor progression *(24)*. In recent studies, the mechanism of this important phenomenon was studied with regard to angiogenesis and other chemical regulators of tumor colonization *(24)*. However, these experimental models did not allow direct observation of the dormant colonies in fresh, live tissue as it occurs over time, as do the GFP studies.

1.7. Genetically Fluorescent Melanoma Bone and Organ Metastasis Models

We have characterized metastatic properties of bright, highly stable GFP-expression transductants of the B16 mouse malignant-melanoma cell line and LOX human melanoma line *(29)*. The highly fluorescent malignant-melanoma cell lines allowed the

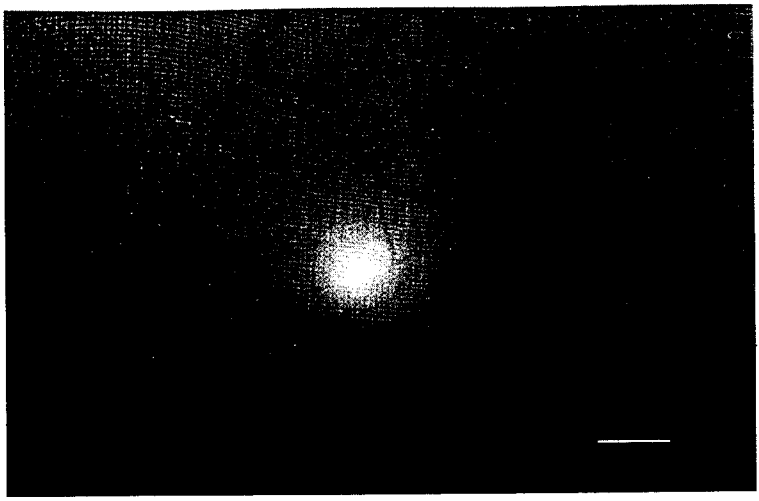

Fig. 5. Brain metastasis of GFP-expressing ANIP-973 human lung-cancer cells 8 wk after tail-vein injection in nude mice *(16)*.

visualization of skeletal and multi-organ metastases after intravenous (iv) injection of B16 cells in C57BL/6 mice and intradermal (id) injection of LOX in nude mice. The melanoma cell lines were transduced with the pLEIN-expression retroviral vector containing the GFP and neomycin resistance genes. Extensive bone (Fig. 6) and bone-marrow metastases of B16F0 were visualized by GFP expression when the animals were sacrificed after 3 wk after cell implantation. This is the first observation of experimental skeletal metastases of melanoma, which was made possible by GFP expression. For both cell lines, metastases were visualized in many other organs, including the brain, lung (Fig. 7), pleural membrane, liver, kidney, adrenal gland, lymph nodes (Fig. 8), muscle, and skin by GFP fluorescence.

1.8. Whole-Body Fluorescence Optical Tumor Imaging of Tumor Growth and Metastasis

Whole-body optical images visualized metastatic lesions of GFP-expressing tumors in the brain, liver (Fig. 9), pancreas, lymph nodes, and bone in transplanted mice. These images were used for real time, quantitative measurement of primary and metastatic tumor growth in each of these organs. Imaging was with either a transilluminated epi-fluorescence microscope or a fluorescence light box and thermoelectrically cooled color charged–coupled device (CCD) camera. The depth to which metastasis and micrometastasis could be imaged depended on their size. The simple, noninvasive, and highly selective imaging of growing tumors, made possible by the strong GFP fluorescence, enabled the detailed visualization of tumor growth and metastasis formation, even in freely moving animals. This new GFP imaging technology will facilitate in vivo high-throughput screening of antitumor and antimetastatic drugs *(25)*.

1.9. Selective In Vivo Tumor Delivery of the Green Fluorescent Protein Gene to Report Future Occurrence of Metastasis

The GFP gene was administered to intraperitoneally growing human stomach cancer in nude mice in order to visualize future regional and distant metastases. GFP retroviral

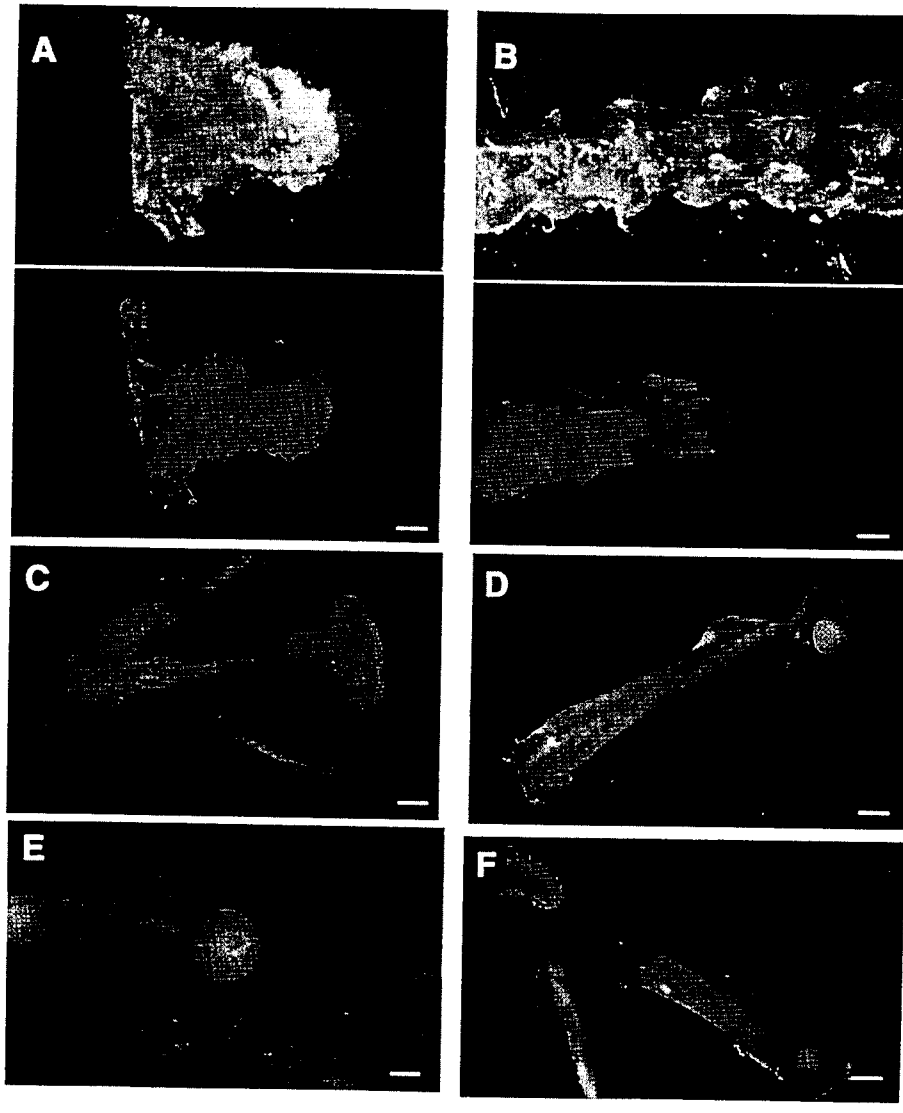

Fig. 6. Bone metastasis of B16F0 GFP C1 visualized by GFP *(29)*.
a: Skull, Top: no metastasis was detected under bright-field microscopy. Bar = 640 μm. Bottom: shows same area as top part, bone metastasis visualized in the skull under fluorescent microscopy.
b: Vertebral body, Top: no metastasis was detected under bright-field microscopy. Bar = 1280 μm. Bottom: shows same area as top part, bone metastasis visualized in the vertebral body under fluorescent microscopy.
c: Bone metastases visualized by GFP expression in humerus and scapula. Bar = 1280 μm.
d: Bone metastases visualized by GFP expression in the distal end of the femur. Bar = 1280 μm.
e: Bone metastases visualized by GFP expression in the head of the femur. Bar = 800 μm.
f: Bone metastases visualized by GFP expression in pelvis. Bar = 1280 μm.

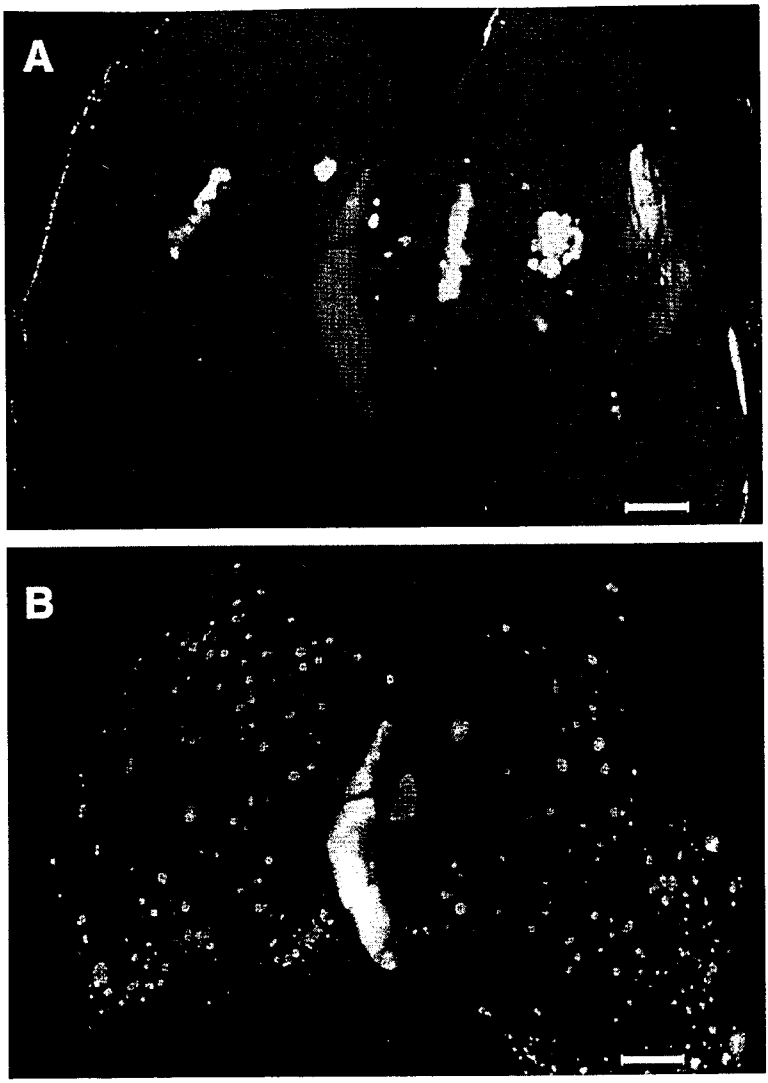

Fig. 7. Lung metastasis of LOX visualized by GFP *(29)*.
a: Shows the surface of the lung of nude mouse. No metastasis was detected under bright-field microscopy. Bar = 1280 μm.
b: Same field as **a.** Numerous micro-metastases and metastases are visualized by GFP expression in the lung under fluorescence microscopy. Bar = 1280 μm.

supernatants were ip-injected from d 4 to d 10 following ip implantation of the cancer cells. Tumor and metastasis fluorescence was visualized every other wk with the use of fluorescence optics via a laparotomy on the tumor-bearing animals. No normal tissues were found to be transduced by the GFP retrovirus. Within 2 wk after retroviral GFP delivery, GFP-expressing tumor cells were observed in gonadal fat, greater omentum, and intestine, indicating that these primary intraperitoneally growing tumors were efficiently transduced by the GFP gene and could be visualized by its expression. At the second and

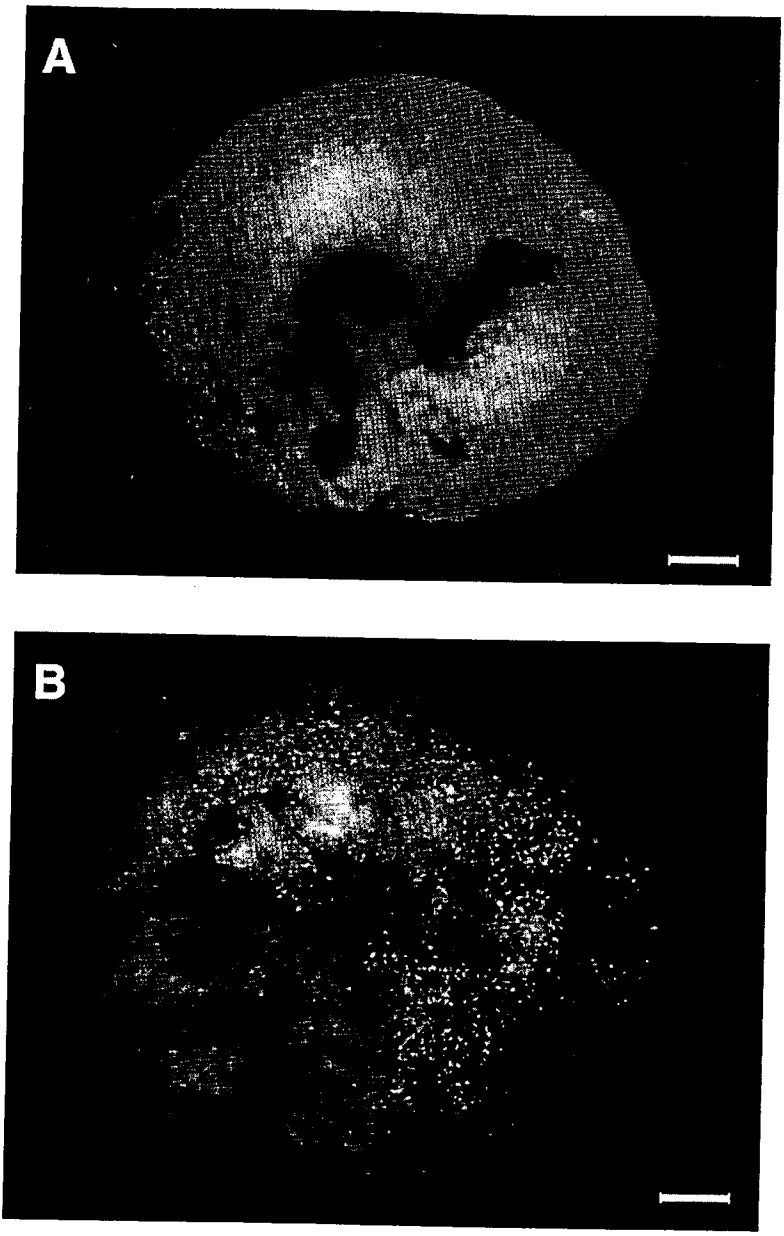

Fig. 8. Lymph-node metastasis of LOX visualized by GFP *(29)*
a and b: Tumor metastasized to the lymph nodes visualized by GFP expression. Bar = 200 μm.

third laparotomies at 4 and 6 wk, respectively, GFP-expressing tumor cells were found spreading to lymph nodes in the mesentery. At the fourth laparotomy at 8 wk, widespread tumor growth including liver metastasis was observed. Thus, reporter-gene transduction of the primary tumor enabled detection of its subsequent metastasis. This gene-therapy model could be applied to primary tumors before resection or other treatment in order to have a fluorescent early detection system for metastasis and recurrence *(26)*.

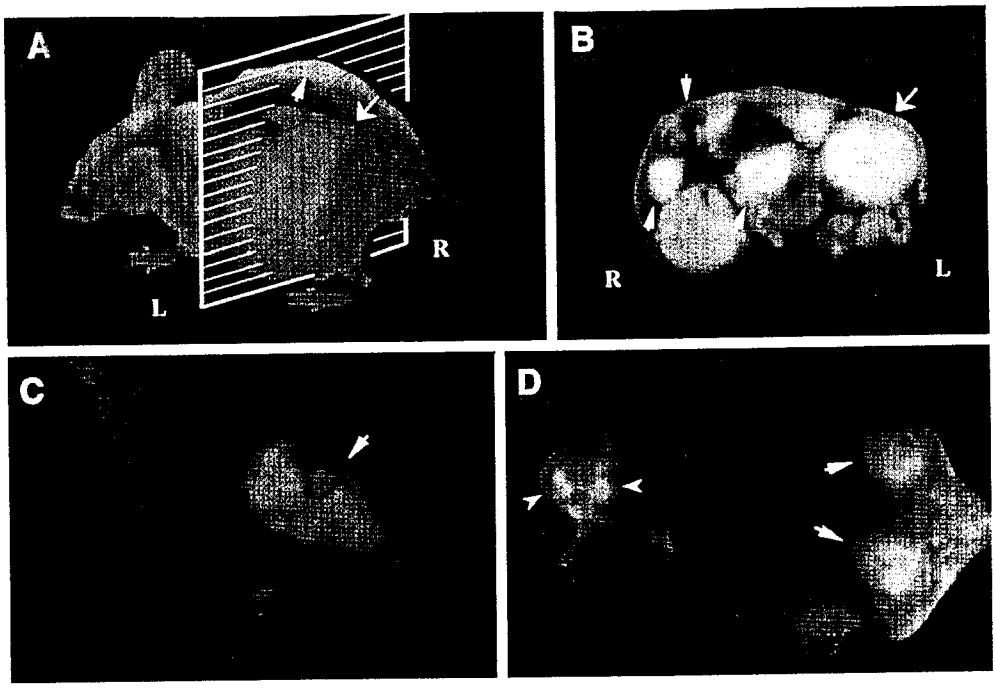

Fig. 9. External and internal images of liver lesions of AC3488-GFP *(25)*.
a: Lateral, whole-body image of metastatic liver lesions of a GFP-expressing human colon cancer in the left and right lobes of a live nude mouse at d 21 after surgical orthotopic transplantation (SOI).
b: Cross-section of mouse shown in Fig. 9A corresponding to the level of the external image of the tumor in the liver that was acquired (Fig. 9A). Arrows show metastatic lesions in the various lobes of the liver.
c: Fluorescent whole-body ventral image of primary colon tumor.
d: Dorsal external image of metastatic tumor in the caudal region of the left and right lobes of the liver (thick arrows), and skull metastasis (arrowheads).

2. METHODS

2.1. Imaging Apparatus

A Leica fluorescence stereo microscope, model LZ12, equipped with a 50W mercury lamp, was used for high-magnification imaging of GFP-expressing tumors and metastasis *in situ* or for whole-body imaging of animals with GFP-expressing tumors. Selective excitation of GFP was produced through a D425/60 band-pass filter and 470 DCXR dichroic mirror. Emitted fluorescence was collected through a long-pass filter GG475 (Chroma Technology, Brattleboro, VT) on a Hamamatsu C5810 3-chip cooled color CCD camera (Hamamatsu Photonics Systems, Bridgewater, NJ). Images were processed for contrast and brightness and analyzed with the use of Image Pro Plus 3.1 software (Media Cybernetics, Silver Springs, MD) Images of 1024 × 724 pixels were captured directly on an IBM PC or continuously through video output on a high-resolution Sony VCR model SLV-R1000 (Sony Corp., Tokyo, Japan). Whole-body imaging that visualized the entire animal at lower magnification was carried out in a light box illuminated by blue light fiberoptics (Lightools Research, Inc., Encinitas, CA) and imaged using the thermoelectrically cooled color CCD camera (*25*).

2.2. Retroviral DNA Expression Vector

The RetroXpress vector pLEIN was purchased from CLONTECH Laboratories, Inc. (Palo Alto, CA). The pLEIN vector expresses enhanced green fluorescent protein (EGFP) and the neomycin resistance gene on the same bicistronic message that contains an internal ribosome entry site (IRES) *(18,19)*.

2.3. Retroviral Production

PT67, an NIH-3T3-derived packaging cell line, expressing the 10-Al viral envelope, was purchased from CLONTECH Laboratories, Inc. PT67 cells were cultured in Dulbecco's Modified Eagle's Medium (DME) (Irvine Scientific, Santa Ana, CA) supplemented with 10% heat-inactivated fetal bovine serum (FBS) (Gemini Bio-products, Calabasas, CA). For vector production, packaging cells (PT67), at 70% confluence, were incubated with a precipitated mixture of DOTAP™ reagent (Boehringer Mannheim), and saturating amounts of pLEIN plasmid for 18 h. Fresh medium was replenished at this time. The cells were examined by fluorescence microscopy after 48 h. For selection of GFP transductants, the cells were cultured in the presence of 500 μg/mL–2000 μg/mL of G418 (Life Technologies, Grand Island, NY) for 7 ds *(18,19)*.

2.4. Retroviral Transduction of Tumor Cells

For GFP gene transduction, 20%-confluent cancer cells were incubated with a 1:1 precipitated mixture of retroviral supernatants of PT67 cells and RPMI-1640 (GIBCO-BRL) containing 10% FBS (Gemini Bio-products, Calabasas, CA) for 72 h. Fresh medium was replenished at this time. Cells were harvested by trypsin/EDTA 72 hs postinfection, and subcultured at a ratio of 1:15 into selective medium containing 200 μg/mL of G418. The level of G418 was gradually increased to 800–1000 μg/mL. Stable GFP-expressing clones were then isolated in the absence of selective agent. Clones expressing GFP were isolated with cloning cylinders (Bel-Art Products, Pequannock, NJ) by trypsin EDTA and were amplified and transferred by conventional culture methods *(18,19)*.

2.5. Subcutaneous Tumor Growth

Three 6-wk-old Balb/c *nu/nu* female mice were injected subcutaneously with a single dose of 10^7 stable GFP transductants. Cells were first harvested by trypsinization, and washed three times with cold serum-containing medium, then kept on ice. Cells were injected in a total vol of 0.4 mL within 40 min of harvesting. The nude mice were sacrificed to harvest the tumor fragments 3 wk after tumor-cell injection *(14–19)*.

2.6. Experimental Metastasis

Nude mice were injected in the tail vein of mice with a single dose of 1×10^7 stable GFP-expressing cancer cells. Cells were first harvested by trypsinization, and washed three times with cold serum-containing medium, then kept on ice. Cells were injected in a total vol of 0.8 mL of serum-free medium within 40 min of harvesting. After various times, the mice were sacrificed, and fresh visceral organs and the skeleton were analyzed by fluorescence microscopy.

2.7. Surgical Orthotopic Implantation

2.7.1 Ovarian Cancer

Tumor fragments (1 mm^3) derived from the nude mouse sc CHO-K1-GFP tumors were implanted by SOI on the ovarian serosa in six nude mice *(14,27)*. The mice were anesthetized by isofluran inhalation. An incision was made through the left lower abdominal pararectal line and peritoneum. The left ovary was exposed, and part of the serosal membrane was scraped with a forceps. Four 1-mm^3 tumor pieces were fixed on the scraped site of the serosal surface with an 8–0 nylon suture (Look, Norwell, MA). The ovary was then returned into the peritoneal cavity, and the abdominal wall and the skin were closed with 6–0 silk sutures. Four weeks later, the mice were sacrificed, and the lungs and the other organs were removed. All procedures of the operation described above were performed with a ×7 magnification microscope (Olympus) *(14)*.

2.7.2. Lung Cancer

Tumor fragments (1 mm^3) derived from the ANIP-GFP or H460-GFP sc tumor growing in the nude mouse were implanted by SOI on the left lung in nude mice *(15,18)*. The mice were anesthetized by isofluran inhalation. The animals were put in a position of right lateral decubitus, with the four limbs restained. A 0.8-cm transverse incision of the skin was made in the left-chest wall. Chest muscles were separated by sharp dissection, and costal and intercostal muscles were exposed. A 0.4–0.5-cm intercostal incision between the third and fourth rib on the chest wall was made, and the chest wall was opened. The left lung was taken up by a forceps and tumor fragments were promptly sewn into the upper lung with one 8–0 suture. The lung was then returned into the chest cavity. The incision in the chest wall was closed by a 6–0 surgical suture. The closed condition of the chest wall was examined immediately, and if a leak existed, it was closed by additional sutures. After closing the chest wall, an intrathoracic puncture was made by using a 3-mL syringe and 25 and II gauge needle to withdraw the remaining air in the chest cavity. After the withdrawal of air, a completely inflated lung could be seen through the thin chest wall of the mouse. Then the skin and chest muscle were closed with a 6–0 surgical suture in one layer. All procedures of the operation described here were performed with a ×7 magnification microscope (Olympus).

2.7.3. Prostate Cancer

Two tumor fragments (1 mm^3) from a high-GFP-fluorescent sc tumor from a single animal were implanted by SOI in the dorsolateral lobe of the prostate in five nude mice *(19)*. After proper exposure of the bladder and prostate following a lower midline abdominal incision, the capsule of the prostate was opened, and the two tumor fragments were inserted into the capsule. The capsule was then closed with an 8–0 surgical suture. The incision in the abdominal wall was closed with a 6–0 surgical suture in one layer *(7,8)*. The animals were kept under isoflurane anesthesia during surgery. All procedures of the operation described here were performed with a × 7 magnification microscope (Olympus).

2.8. Analysis of the GFP-fluorescent Metastases at Autopsy

Mice were sacrificed when their performance status began to decline and the systemic organs were removed. The orthotopic primary tumor and all major organs, as well as the whole skeleton, were explored *in situ* by fluorescence microscopy. The

fresh samples were then sliced at approx 1-mm thickness and further observed under fluorescence microscopy.

REFERENCES

1. Lin WC, Pretlow TP, Pretlow TG, Culp LA. Bacterial lacZ gene as a highly sensitive marker to detect micrometastasis formation during tumor progression. *Cancer Res* 1990; 50: 2808–2817.
2. Lin WC, Culp LA. Altered establishment/clearance mechanisms during experimental micrometastasis with live and/or disabled bacterial lacZ-tagged tumor cells. *Invasion Metastasis* 1992; 12: 197–209.
3. Morin J, Hastings J. Energy transfer in a bioluminescent system. *J Cell Physiol* 1971; 77: 313–318.
4. Chalfie M, Tu Y, Euskirchen G, Ward WW, Prasher DC. Green fluorescent protein as a marker for gene expression. *Science* 1994; 263: 802–805.
5. Cheng L, Fu J, Tsukamoto A, Hawley RG. Use of green fluorescent protein variants to monitor gene transfer and expression in mammalian cells. *Nat Biotechnol* 1996; 14: 606–609.
6. Prasher DC, Eckenrode VK, Ward WW, Prendergast FG, Cormier MJ. Primary structure of the *Aequorea victoria* green-fluorescent protein. *Gene* 1992; 111: 229–233.
7. Yang F, Moss LG, Phillips GN Jr. The molecular structure of green fluorescent protein. *Nat Biotechnol* 1996; 14: 1246–1251.
8. Cody CW, Prasher DC, Welstler VM, Prendergast FG, Ward WW. Chemical structure of the hexapeptide chromophore of the *Aequorea* green fluorescent protein. *Biochemistry* 1993; 32: 1212–1218.
9. Heim R, Cubitt AB, Tsien RY. Improved green fluorescence. *Nature* 1995; 373: 663–664.
10. Delagrave S, Hawtin RE, Silva CM, Yang MM, Youvan DC. Red-shifted excitation mutants of the green fluorescent protein. *Bio/Technology* 1995; 13: 151–154.
11. Cormack B, Valdivia R, Falkow S. FACS-optimized mutants of the green fluorescent proten (GFP). *Gene* 1996; 173: 33–38.
12. Crameri A, Whitehorn EA, Tate E, Stemmer WPC. Improved green fluorescent protein by molecular evolution using DNA shuffling. *Nat Biotechnol* 1996; 14: 315–319.
13. Zolotukhin S, Potter M, Hauswirth WW, Guy J, Muzycka N. 'Humanized' green fluorescent protein cDNA adapted for high-level expression in mammalian cells. *J Virology* 1996; 70: 4646–4654.
14. Chishima T, Miyagi Y, Wang X, Yamaoka H, Shimada H, Moossa AR, et al. Cancer invasion and micrometastasis visualized in live tissue by green fluorescent protein expression. *Cancer Res* 1997; 57: 2042–2047.
15. Chishima T, Miyagi Y, Wang X, Baranov, E, Tan Y, Shimada H, et al. Metastatic patterns of lung cancer visualized live and in process by green fluorescent protein expression. *Clinical & Experimental Metastasis* 1997; 15: 547–552.
16. Chishima T, Miyagi Y, Wang X, Tan Y, Shimada H, Moossa AR, et al. Visualization of the metastatic process by green fluorescent protein expression. *Anticancer Res* 1997; 17: 2377–2384.
17. Chishima T, Miyagi Y, Li L, Tan Y, Baranov E, Yang M, et al. The use of histoculture and green fluorescent protein to visualize tumor cell host interaction. *In Vitro Cell Dev Biol* 1997; 33: 745–747.
18. Yang M, Hasegawa S, Jiang P, Wang X, Tan Y, Chishima T, et al. Widespread skeletal metastatic potential of human lung cancer revealed by green fluorescent protein expression. *Cancer Res* 1998; 58: 4217–4221.
19. Yang M, Jiang P, Sun FX, Hasegawa S, Baranov E, Chishima T, et al. A fluorescent orthotopic bone metastasis model of human prostate cancer. *Cancer Res* 1999; 59: 781–786.
20. Kaufman RJ, Davies MV, Wasley LC, Michnick D. Improved vectors for stable expression of foreign genes in mammalian cells by use of the untranslated leader sequence from EMC virus. *Nucleic Acids Res* 1991; 19: 4485–4490.
21. Astoul P, Colt HG, Wang X, Hoffman RM. A "patient-like" nude mouse model of parietal pleural human lung adenocarcinoma. *Anticancer Res* 1994; 14: 85–92.
22. Wang X, Fu X, Hoffman RM. A new patient-like metastatic model of human lung cancer constructed orthotopically with intact tissue via thoracotomy in immunodeficient mice. *Int J Cancer* 1992; 51: 992–995.
23. Yang M, Chishima T, Wang X, Baranov E, Shimada H, Moossa AR, et al. Multi-organ metastatic capability of Chinese ovary cells revealed by green fluorescent protein (GFP) expression. *Clin and Exp Metastasis* 1999; 17: 417–422.
24. Holmgren L, O'Reilly MS, Folkman J. Dormancy of micrometastases: balanced proliferation and apoptosis in the presence of angiogenesis suppression. *Nat Med* 1995; 1: 149–153.

25. Yang M, Baranov E, Jiang P, Sun F-X, Li X-M, Li L, et al. Whole-body optical imaging of green fluorescent protein-expressing tumors and metastases. *Proc Natl Acad Sci USA* 2000; 97: 1206–1211.
26. Hasegawa S, Yang M, Chishima T, Shimada H, Moossa AR, Hoffman RM. *In vivo* tumor delivery of the green fluorescent protein gene to report future occurrence of metastasis. *Cancer Gene Ther* 2000; 7: 1336–1340.
27. Fu X, Hoffman RM. Human ovarian carcinoma metastatic models constructed in nude mice by orthotopic transplantation of histologically-intact patient specimens. *Anticancer Res* 1993; 13: 283–286.
28. Naumov GN, Wilson SM, MacDonald IC, Schmidt EE, Morris V, Groom AC, et al. Cellular expression of green fluorescent protein, coupled with high-resolution *in vivo* videomicroscopy, to monitor steps in tumor metastasis. *J Cell Sci* 1999; 112 (12): 1835–1842.
29. Yang M, Jiang P, An Z, Baranov E, Li L, Hasegawa S, et al. Genetically fluorescent melanoma bone and organ metastasis models. *Clin Can Res* 1999; 5: 3549–3559.